Multi-component orbital interactions during oxyacyl radical addition reactions involving imines and electron-rich olefins†

Sara H. Kyne,[a,b] Carl H. Schiesser*[a,b] and Hiroshi Matsubara[c]

Received 17th September 2007, Accepted 5th October 2007
First published as an Advance Article on the web 2nd November 2007
DOI: 10.1039/b714324a

Ab initio and DFT calculations reveal that oxyacyl radicals add to imines and electron-rich olefins through simultaneous SOMO–π*, SOMO–π and π*–HOMO interactions between the radical and the radicalophile. At the BHandHLYP/aug-cc-pVDZ level, energy barriers of 20.3 and 22.0 kJ mol^{-1} are calculated for the attack of methoxycarbonyl radical at the carbon and nitrogen ends of methanimine, respectively. In comparison, barriers of 22.0 and 8.6 kJ mol^{-1} are calculated at BHandHLYP/aug-cc-pVDZ for reaction of methoxycarbonyl radical at the 1- and 2-positions in aminoethylene, respectively. Natural bond orbital (NBO) analysis at the BHandHLYP/6-311G** level of theory reveals that SOMO–π*, SOMO–π and π*–LP interactions are worth 111, 394 and 55 kJ mol^{-1} respectively in the transition state (**8**) for reaction of oxyacyl radical at the nitrogen end of methanimine; similar interactions are observed for the chemistry involving aminoethylene. These multi-component interactions are responsible for the unusual motion vectors associated with the transition states involved in these reactions.

Introduction

Methods of generating carbon-centred radicals from alcohols are important tools for the synthetic chemist.[1] Some time ago, we demonstrated that aryltelluroformates **1** are photochemically and thermally labile and are effective precursors of oxyacyl radicals **2** that, depending on reaction conditions, can decarboxylate to afford alkyl radicals (Scheme 1) or can be trapped with reagents such as diphenyl diselenide or through cyclization to afford novel heterocycles such as **3** (Scheme 2).[2] Aryltelluroformates, therefore, provide an alternative method for the deoxygenation of alcohols that can be useful in systems where more traditional precursors such as xanthates[3] undergo competitive ionic rearrangement.[4]

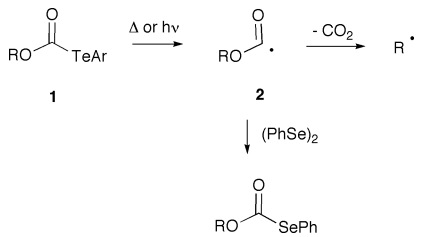

Scheme 1

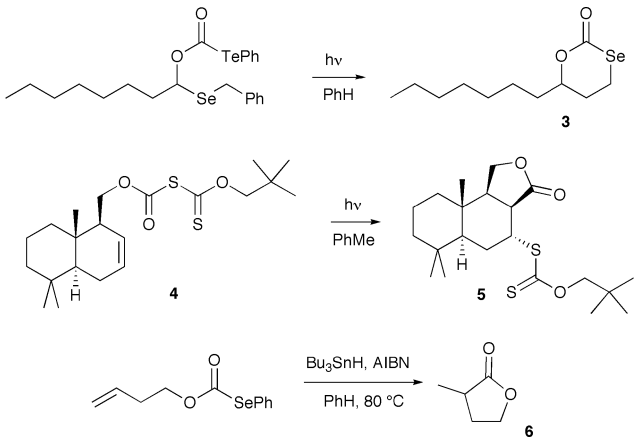

Scheme 2

Oxyacyl radicals are intermediates that can also be used during the preparation of lactones and related compounds, however their synthetic use has not been exploited to any great extent. Some examples of the synthetic utility of oxyacyl radicals are shown in Scheme 2.[2,5,6]

Xanthates can be used to generate both acyl and oxyacyl radicals, with the addition of these radicals to olefins yielding species such as ketones and esters. The *S*-alkoxycarbonyl xanthate **4**, upon photolysis, affords xanthate **5** through a process involving 5-*exo* cyclisation of an oxyacyl radical. Upon treatment of **5** with 1,8-diazabicyclo[5.4.0]undec-7-ene (DBU), racemic cinnamolide was isolated.[5]

Unlike their tellurium counterparts, selenoformates react under standard radical conditions to afford oxyacyl radicals that have been used for a variety of synthetic purposes including the synthesis of lactones such as **6**.[6]

Recently, we reported that acyl radicals can masquerade as electrophiles through multi-component orbital interactions and

[a]*School of Chemistry, The University of Melbourne, Victoria, Australia 3010*
[b]*Bio21 Molecular Science and Biotechnology Institute, The University of Melbourne, Victoria, Australia 3010. E-mail: carlhs@unimelb.edu.au; Fax: +61 3 9347 8189; Tel: +61 3 8344 2432*
[c]*Department of Chemistry, Graduate School of Science, Osaka Prefecture University, Sakai, Osaka 599-8531, Japan*

† Electronic supplementary information (ESI) available: Optimised geometries (Gaussian archive entries) of structures **7–10** at all levels of theory used in this study. UHF/6-311G** calculated energy barriers $\Delta E^{1\ddagger}$–$\Delta E_4^{\ddagger}$ for reactions depicted in Schemes 4 and 5. GaussView generated animations of the transition state vectors in **7**, **8**, **9** (R = NH_2) and **10** (R = NH_2) as Audio Video Interleave (AVI) files. See DOI: 10.1039/b714324a

that these interactions are responsible for the unexpected selectivity often observed for reactions involving these radicals.[7,8] For example, acyl radicals are N-philic;[8,9] that is they prefer to cyclize at the nitrogen end of imine π-systems irrespective of Beckwith–Houk[10] considerations (Scheme 3). This selectivity can be explained through consideration of multi-component orbital interactions (Scheme 3).[11]

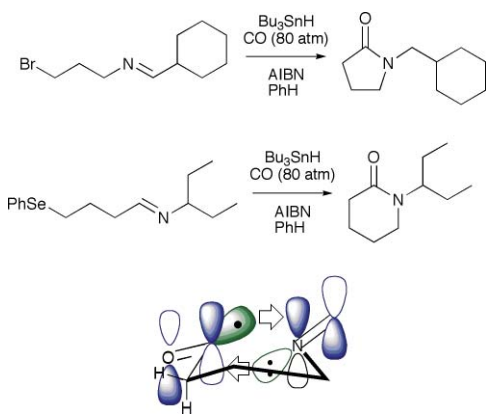

Scheme 3

With our continuing interest in oxyacyl radicals and multi-component orbital interactions in radical chemistry, we chose to explore by computational techniques whether or not similar interactions exist for chemistry involving oxyacyl radicals. We now report that, like their acyl counterparts, these radicals also exhibit multi-component orbital interactions when confronted by imines and electron-rich olefins.

Results and discussion

Reaction of methoxycarbonyl radical with methanimine

We began this investigation by examining the reaction of methoxycarbonyl radical with methanimine, as representative examples of the key reacting components. As previous benchmark studies had established that BHandHLYP is a reliable method for the study of acyl and related radical chemistry,[7,12] we chose to primarily use this method in this study. Searching of the $C_3H_6NO_2$ potential energy surface located structures **7** and **8** as the lowest energy transition states for reaction of methoxycarbonyl radical at the carbon and nitrogen ends of the C=N bond in methanimine, respectively (Scheme 4), and are displayed in Fig. 1, along with important geometrical features. Motion arrows associated with the transition state vector in each case are included and give insight into the

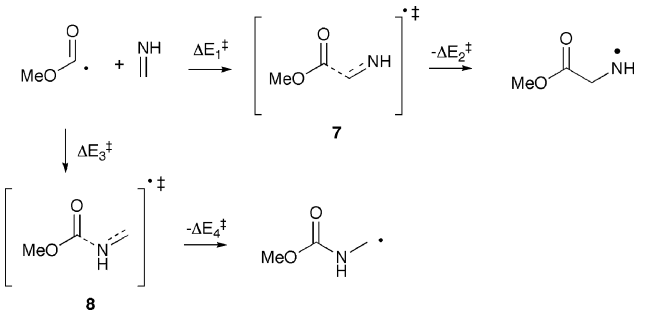

Scheme 4

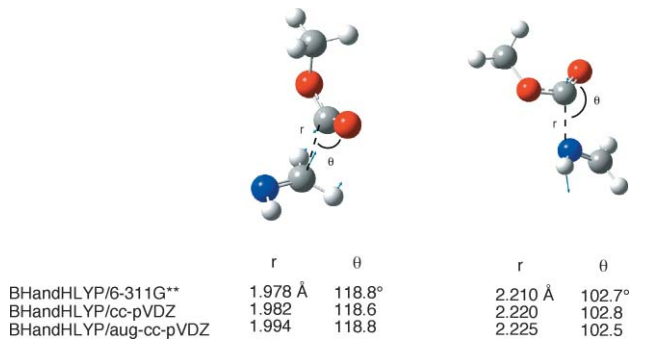

Fig. 1 Key calculated structural parameters for transition states **7** (left) and **8** (right).

attack trajectory of methoxycarbonyl radical during addition to the imine.‡ In particular, transition state **8** displays similar rocking motion§ (ν = 464i cm^{-1}, BHandHLYP/6-311G**) to its acetyl counterpart.[7]

Transition state separations are observed to be smaller for attack at the carbon end of the imine bond, with transition state **7** predicted to have separations between about 1.97–1.99 Å, compared to transition state **8** with separations of 2.21–2.23 Å, and are very similar to those calculated for the analogous transition states involving acetyl radical.[7]

Activation energy data (Scheme 4, $\Delta E_1^{\ddagger}$–$\Delta E_4^{\ddagger}$) calculated at various levels of theory are listed in Table 1 and reveal that at the BHandHLYP/aug-cc-pVDZ level of theory, addition to the carbon end of the π-bond (transition state **7**), has a $\Delta E_1^{\ddagger}$

‡ Animations of the transition state imaginary frequency are conveniently visualised using the GaussView software that complements Gaussian 03.[14] BHandHLYP/6-311G** generated animations of the transition state vectors in **7**, **8**, **9** (R = NH_2) and **10** (R = NH_2) are available in the ESI† as Audio Video Interleave (AVI) files.

§ When the transition state vector is animated using software such as GaussView.

Table 1 Calculated energy barriers[a] for the forward ($\Delta E_1^{\ddagger}$, $\Delta E_3^{\ddagger}$) and reverse ($\Delta E_2^{\ddagger}$, $\Delta E_4^{\ddagger}$) reactions of methoxycarbonyl radical with methanimine and imaginary frequencies (ν)[b] of transition states **7** and **8** (Scheme 4)

	7					**8**				
Method	$\Delta E_1^{\ddagger}$	$\Delta E_1^{\ddagger}$ + ZPE	$\Delta E_2^{\ddagger}$	$\Delta E_2^{\ddagger}$ + ZPE	ν	$\Delta E_3^{\ddagger}$	$\Delta E_3^{\ddagger}$ + ZPE	$\Delta E_4^{\ddagger}$	$\Delta E_4^{\ddagger}$ + ZPE	ν
BHandHLYP/6-311G**	21.8	25.5	147.4	141.0	385i	19.7	23.7	204.4	197.5	464i
BHandHLYP/cc-pVDZ	20.1	23.7	152.9	146.1	373i	17.3	21.4	206.1	198.7	453i
BHandLYP/aug-cc-pVDZ	20.3	24.1	149.4	143.1	363i	22.0	26.1	204.7	198.8	433i

[a] Energies in kJ mol^{-1}. [b] Frequencies in cm^{-1}.

calculated to be 20.3 kJ mol^{-1}. This energy is only marginally lower than that of its rival (transition state **8**), with a $\Delta E_3^{\ddagger}$ calculated to be 25.0 kJ mol^{-1}, indicating a slight preference for addition to the carbon end of the imine. To the best of our knowledge, there are no reports of either inter- or intramolecular oxyacyl addition reactions with imines to compare our calculated results with. However, our data can be compared with calculated activation energies of 20 and 25 kJ mol^{-1} for the analogous reactions involving acetyl radicals at the same level of theory,[7] and 32 and 50 kJ mol^{-1} for methyl radical addition at the carbon and nitrogen ends of methanimine respectively using G2//MP2(full)/6-311G*.[13] Clearly, methoxycarbonyl radical has a significantly greater preference for addition to nitrogen than does methyl radical and this preference can be understood through application of natural bond orbital (NBO) analysis (*vide infra*).

Table 1 also shows that the calculated energy barriers for the reverse reactions (Scheme 4, $\Delta E_2^{\ddagger}$, $\Delta E_4^{\ddagger}$) are substantially different for fragmentation at the two ends of the carbon–nitrogen bond, with preference for fragmentation through transition state **7** to be consistently of lower energy. At the BHandHLYP/aug-cc-pVDZ level of theory these energy barriers are calculated to be 149.4 and 204.7 kJ mol^{-1} for transition states **7** and **8** respectively. Clearly there is substantial preference for the forward reaction in both cases, however the energy barrier is also significantly lower for fragmentation of the product radical through transition state **7** when compared to **8** and this is a reflection on the relative stabilities of nitrogen *versus* carbon-centered radicals.

Representative orbital energy interaction diagrams for transition states **7** and **8** are shown in Fig. 2 and natural bond orbital (NBO) analysis at the BHandHLYP/6-311G** level of theory was carried out for these two structures. In the case of addition to the carbon end of the imine (transition state **7**), this analysis reveals interactions between the unpaired methoxycarbonyl radical (SOMO) and the imine π and π* orbitals (Fig. 2, left). The SOMO–π* interaction, calculated to be worth 130 kJ mol^{-1}, is evident in the α spin-set, with the SOMO–π interaction evident in the β spin-set and calculated to contribute 137 kJ mol^{-1} (Fig. 2, **7a**, **7b**). The nitrogen lone pair (calculated to be the HOMO) is orientated in such a manner as to make itself unavailable for bonding, and therefore does not contribute to the developing bonding interactions when methoxycarbonyl radical attacks the carbon end of methanimine. With the SOMO–π* interaction similar in energy to the SOMO–π interaction, we can conclude

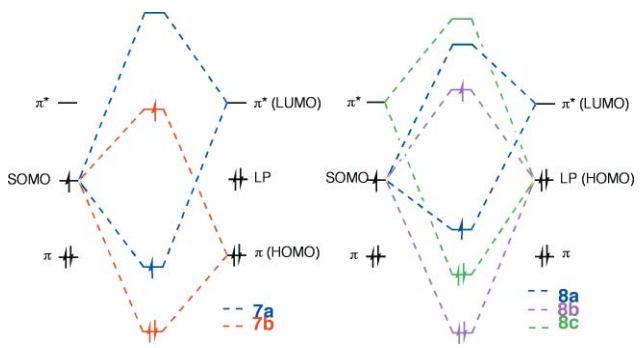

Fig. 2 Representative energy diagrams for orbital interactions involved in the homolytic addition of methoxycarbonyl radical to methanimine *via* transition states **7** (left) and **8** (right).

that in its reaction at the carbon end of the imine methoxycarbonyl radical acts as an ambiphilic radical.¶ Visualisation of the Kohn–Sham orbitals generated at the same level of theory depict the overlap of the two reacting units in transition state **7** (Fig. 3, left).

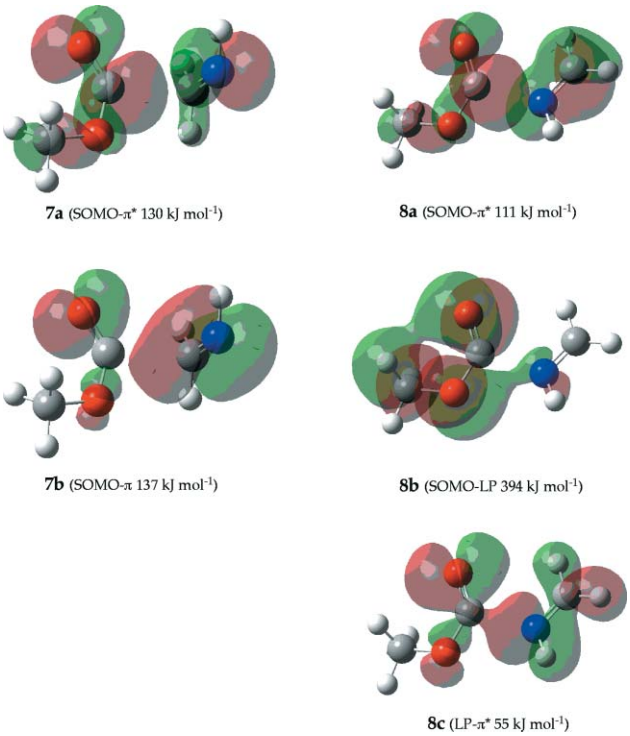

Fig. 3 BHandHLYP/6-311G** calculated Kohn–Sham orbitals involved in transition states **7** (left) and **8** (right).

In comparison, NBO analysis for attack of methoxycarbonyl radical at the nitrogen end of the imine reveals a SOMO–π* interaction worth 111 kJ mol^{-1} in the α spin-set (Fig. 2, **8a**). However, unlike attack at the carbon end of the imine, a strong interaction between the unpaired methoxycarbonyl radical (SOMO) and the lone pair on the nitrogen (imine HOMO) is observed in the β spin-set. The latter interaction is calculated to be approximately four times larger than the SOMO–π* interaction (394 kJ mol^{-1}, Fig. 2, **8b**). Consequently, these data suggest that methoxycarbonyl radical is acting predominantly as an electrophilic radical in its reaction with the imine at the nitrogen end of the π-bond. Of significance is the calculation of a third strong interaction involving the nitrogen lone pair and the π* orbital of the carbonyl π-system. This secondary interaction is apparent in both the α and β spin-sets, is worth 55 kJ mol^{-1}, and is responsible for the unusual transition state motion vectors in transition state **8** (Fig. 2, **8c**). Inspection of the Kohn–Sham orbital associated with this interaction reveals these secondary interactions complement the primary radical interactions and exist in order to derive maximum energy gain from the available orbitals (Fig. 3, right).

¶ The term "ambiphilic radical" was first coined by Beranek and Fischer[16] to describe radicals that exhibit rate enhancements in addition reactions to both electron-rich and electron-poor alkenes. From a frontier MO perspective, the SOMO–π and SOMO–π* interactions in the reaction transition state are similar for these radicals. For examples, see ref. 1.

Table 2 Calculated energy barriers[a] for the forward ($\Delta E_1^{\ddagger}$, $\Delta E_3^{\ddagger}$) and reverse ($\Delta E_2^{\ddagger}$, $\Delta E_4^{\ddagger}$) reactions of methoxycarbonyl radical with ethylene, aminoethylene and 3,3,3-trifluoropropene and imaginary frequencies (ν)[b] of transition states **9** and **10** (Scheme 5)

	9					**10**				
R = H	$\Delta E_1^{\ddagger}$	$\Delta E_1^{\ddagger}$ + ZPE	$\Delta E_2^{\ddagger}$	$\Delta E_2^{\ddagger}$ + ZPE	ν	$\Delta E_3^{\ddagger}$	$\Delta E_3^{\ddagger}$ + ZPE	$\Delta E_4^{\ddagger}$	$\Delta E_4^{\ddagger}$ + ZPE	ν
BHandHLYP/6-311G**	20.6	23.1	145.5	139.5	364i	—	—	—	—	—
BHandHLYP/cc-pVDZ	18.7	21.2	150.5	144.5	347i	—	—	—	—	—
BHandLYP/aug-cc-pVDZ	19.4	22.2	149.2	143.4	345i	—	—	—	—	—
R = NH_2										
BHandHLYP/6-311G**	7.5	11.7	144.0	136.0	349i	20.1	22.6	121.9	115.4	442i
BHandHLYP/cc-pVDZ	6.7	10.7	149.5	141.7	345i	17.4	19.8	126.1	119.7	419i
BHandLYP/aug-cc-pVDZ	8.6	12.6	147.7	139.8	305i	22.0	24.6	124.7	118.3	420i
R = CF_3										
BHandHLYP/6-311G**	14.1	16.1	150.0	144.1	308i	25.5	26.8	137.3	131.7	336i
BHandHLYP/cc-pVDZ	12.5	14.4	154.8	148.9	302i	23.1	24.4	141.1	135.6	326i
BHandLYP/aug-cc-pVDZ	15.8	17.8	154.1	148.1	293i	28.1	29.7	140.3	134.8	328i

[a] Energies in kJ mol^{-1}. [b] Frequencies in cm^{-1}.

Reactions of methoxycarbonyl radical with alkenes

In order to further probe the electron demand in reactions involving oxyacyl radicals, we next turned our attention to the reaction of oxyacyl radical with ethylene and substituted alkenes of varying electron demand that include aminoethylene and 3,3,3-trifluoropropene (Scheme 5). Searching of the relevant potential energy surfaces located transition state structures **9** and **10** for the addition to the two ends of the alkene. The calculated energy barriers for the forward ($\Delta E_1^{\ddagger}$, $\Delta E_3^{\ddagger}$) and reverse ($\Delta E_2^{\ddagger}$, $\Delta E_4^{\ddagger}$) reactions (Scheme 5) and (imaginary) transition state vibrational frequencies are listed in Table 2, while Fig. 4 displays the optimized structures for **9** and **10** together with selected geometric data.

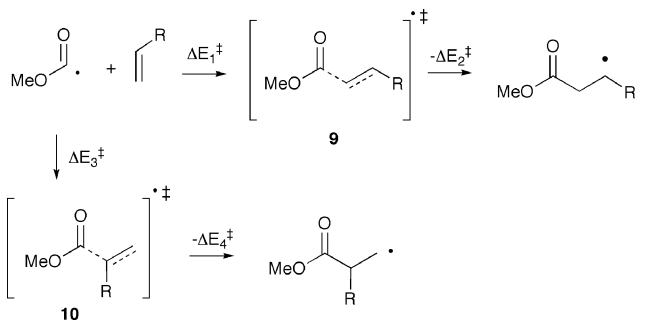

Scheme 5

Inspection of Table 2 reveals that at the BHandHLYP/aug-cc-pVDZ level of theory the energy barriers for the forward and reverse reactions involving ethylene are 19.4 and 149.2 kJ mol^{-1} respectively. Clearly there is substantial preference for the reaction leading to the product in this case. The motion arrows associated with transition state **9** (R = H) (Fig. 4) reveal no unusual transition state motion, and this is perhaps not unexpected.

However, with an electron-donating group present, as in the case of aminoethylene (R = NH_2), we begin to observe the "rocking" motion that we saw for **8**.§ Table 2 reveals that the calculated activation energies for the forward addition reaction (Scheme 5, $\Delta E_1^{\ddagger}$) are consistently lower for attack at the carbon remote from the substituent (transition state **9**) at the various levels of theory employed in this study. At the BHandHLYP/aug-cc-pVDZ level of theory, addition to this end of the π bond, with $\Delta E_1^{\ddagger}$ calculated to be 8.6 kJ mol^{-1}, is approximately 15 kJ mol^{-1} lower than that of its

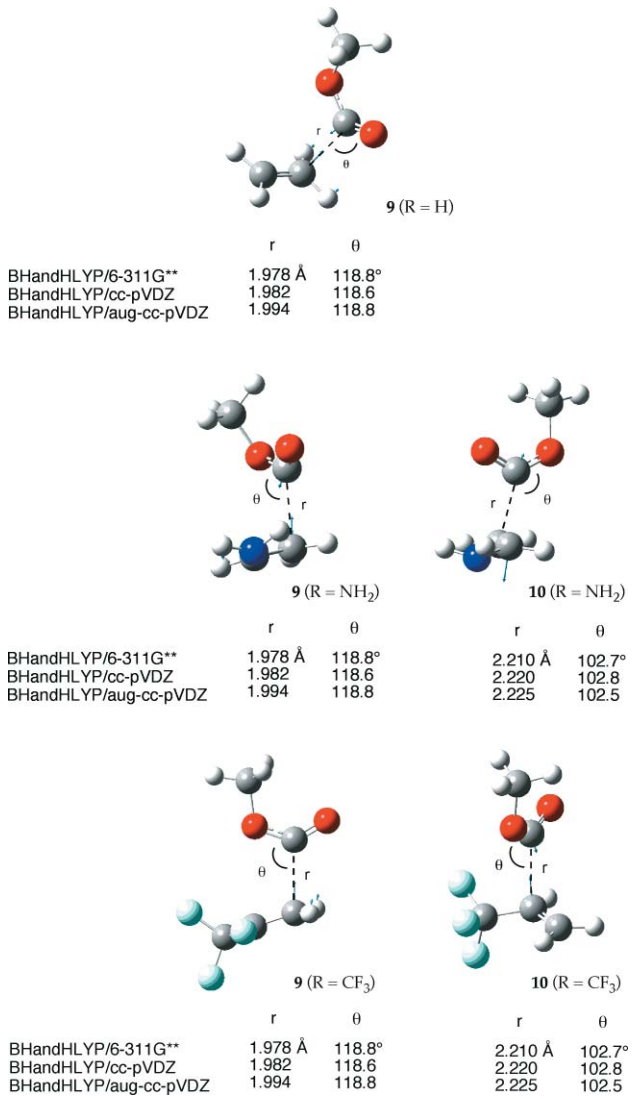

Fig. 4 Key calculated structural parameters for transition states **9** (left) and **10** (right).

counterpart ($\Delta E_3^{\ddagger}$) indicating a clear preference in the distribution of products.

Inclusion of the electron-withdrawing substituent (R = CF_3), while revealing a similar energy trend (Table 2), is not associated with a transition state with unusual motion vectors (Fig. 4). It should be noted that compared to ethylene, both donating and withdrawing groups reduce the energy barrier for attack at the carbon remote from the substituent, suggesting that methoxycarbonyl radical has ambiphilic tendencies.

A representative orbital energy interaction diagram for transition states **9** and **10** is shown in Fig. 5 and NBO analyses were performed at the BHandHLYP/6-311G** level of theory on these structures. Inspection of the NBO data reveals interactions between the oxyacyl radical (SOMO) and the alkene π-system (Fig. 5), as well as, in the case of aminoethylene, further interactions. For the reaction involving ethylene, the SOMO–π* interaction, calculated to be worth 91.3 kJ mol^{-1}, is apparent in the α spin-set, with a contribution of 170 kJ mol^{-1} in the β spin-set from the SOMO–π interaction (Fig. 6). Methoxycarbonyl radical is therefore predicted to be substantially electrophilic in its reaction with ethylene. Visualisation of the Kohn–Sham orbitals generated at the BHandHLYP/6-311G** level of theory allows us to observe the "traditional" transition state for homolytic addition to a π-system (Fig. 6). The conformation assumed in the transition state allows optimum overlap between the radical SOMO and the alkene π-bond.

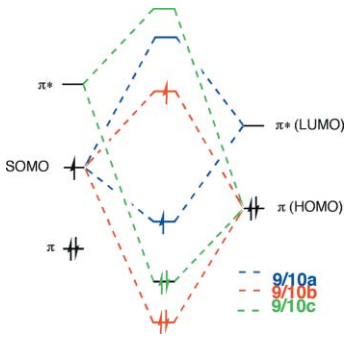

Fig. 5 Representative energy diagram for orbital interactions involved in the homolytic addition of methoxycarbonyl radical to ethylene, aminoethylene and 3,3,3-trifluoropropene *via* transition states **9** and **10**.

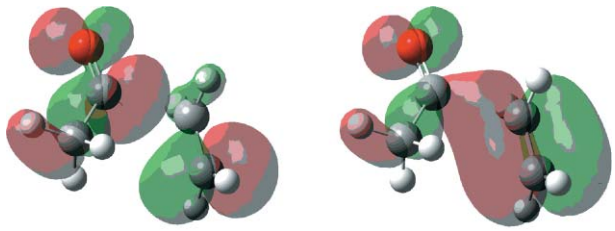

Fig. 6 BHandHLYP/6-311G** calculated Kohn–Sham orbitals involved in transition state **9** (R = H).

NBO analyses for transition states involving aminoethylene (R = NH_2) also reveal interactions between the unpaired oxyacyl radical (SOMO) and the alkene π and π* orbitals (Fig. 7). In the case of addition to the carbon remote from the amine group (transition state **9**), the SOMO–π* interaction, calculated to be worth 68.6 kJ mol^{-1}, is evident in the α spin-set (Fig. 7, **9a**, R = NH_2), with the SOMO–π interaction evident in the β spin-set and calculated to contribute 240 kJ mol^{-1} (Fig. 7, **9b**, R = NH_2). A

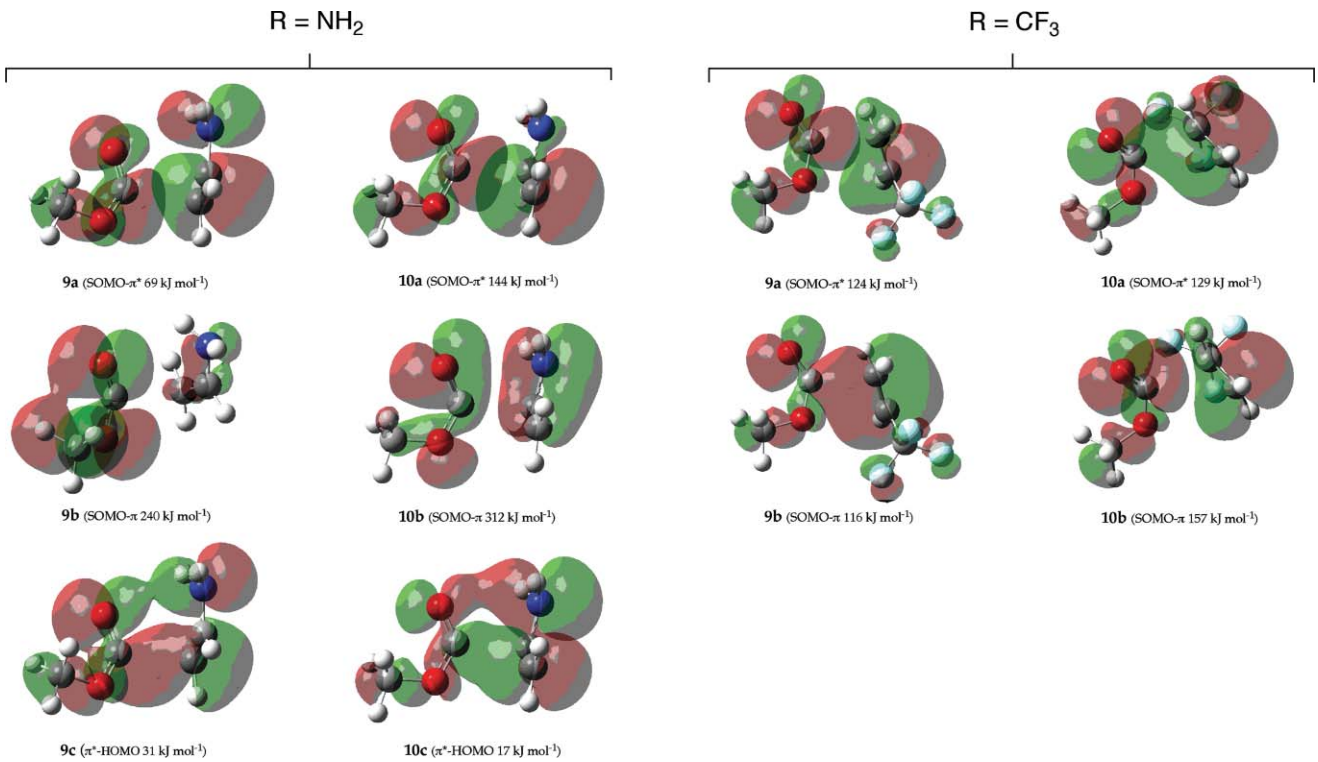

Fig. 7 BHandHLYP/6-311G** calculated Kohn–Sham orbitals involved in transition states **9** and **10**, R = NH_2, CF_3.

third interaction between the π* orbital of the carbonyl π-system and the alkene π-orbital, calculated to be worth 31.1 kJ mol^{-1} is observed in both the α and β spin-sets, and is responsible for the slight rocking motion in transition state **9** (Fig. 7, **9c**, R = NH_2). The same trend is observed for oxyacyl radical addition to the carbon adjacent to the substituent. The SOMO–π interaction evident in the β spin-set is once again calculated to be larger than the SOMO–π* interaction apparent in the α spin-set (312 kJ mol^{-1} *vs.* 144 kJ mol^{-1}). Here, the third interaction (π*–HOMO) is once again observed, calculated to contribute 17.1 kJ mol^{-1} (Fig. 7, **10c**, R = NH_2). In both instances methoxycarbonyl radical is observed to act predominantly as an electrophilic radical in its reaction with aminoethylene.

NBO analysis of the dominant interactions in the transition states involved in the addition of methoxycarbonyl radical to 3,3,3-trifluoropropene reveals a larger contribution from the radical SOMO interaction than in the previous examples. At the BHandHLYP/6-311G** level of theory the transition state SOMO–π* interaction (**9a** = 124 kJ mol^{-1}, **10a** = 129 kJ mol^{-1}) observed in the α spin-set is calculated to be larger than the SOMO–π interaction observed in the β spin-set (Fig. 7) in the case of transition state **9**, but not in the case of transition state **10** (**9b** = 116 kJ mol^{-1}, **10b** = 157 kJ mol^{-1}).

Conclusions

This computational study has shown that oxyacyl radicals add to imines and electron-rich olefins through simultaneous SOMO–π*, SOMO–π and π*–HOMO interactions between the radical and the radicalophile. These multi-component interactions are responsible for the unusual motion vectors associated with the transition states involved in these reactions. Natural bond orbital analyses on the transition states involved in this study provide quantitative information relating to these multi-component interactions. These data also reveal that methoxycarbonyl radical reacts mostly as an electrophilic radical; indeed, comparison with available data for similar reactions involving acetyl radical[7] suggests that oxyacyl radicals are more electrophilic in character than corresponding acyl radicals in their reactions with imines and alkenes.

Computational chemistry

Ab initio and DFT molecular orbital calculations were carried out on Dell PowerEdge 400SC and TX7/i9510 Itanium 2 computers using the Gaussian 03 program.[14] Geometry optimizations were performed using standard gradient techniques using restricted and unrestricted methods for closed- and open-shell systems respectively. In every case, standard basis sets were used. All ground and transition states were verified by vibrational frequency analysis. Values of $<s^2>$ never exceeded 0.82 before annihilation of quartet contamination (except for some UHF calculations). Zero-point vibrational energy (ZPE) corrections have been applied in all cases. Natural bond orbital (NBO) analyses were carried out using *NBO 5.0*[15] linked through the Gaussian 03 program. Optimized geometries and energies for all transition state structures in this study (Gaussian archive entries) are available as part of the ESI.†

Acknowledgements

This work would not have been possible without the generous support of the Australian Research Council through the Centers of Excellence Program. We also gratefully acknowledge the support of the Victorian Institute for Chemical Sciences High Performance Computing Facility and the Library and Science Information Center, Osaka Prefecture University.

Notes and references

1 P. Renaud and M. P. Sibi, *Radicals in Organic Synthesis*, Wiley-VCH, Weinheim, Germany, 2001; vol. 1 and 2.
2 M. A. Lucas and C. H. Schiesser, *J. Org. Chem.*, 1996, **61**, 5754; M. A. Lucas and C. H. Schiesser, *J. Org. Chem.*, 1998, **63**, 3032.
3 D. H. R. Barton and S. W. McCombie, *J. Chem. Soc., Perkin Trans. 1*, 1975, 1574.
4 D. Crich, *Tetrahedron Lett.*, 1988, **20**, 5805.
5 S. Z. Zard, J. R. Forbes and R. N. Saicic, *Tetrahedron*, 1999, **55**, 3791.
6 E. Bosch and M. Bachi, *J. Org. Chem.*, 1992, **57**, 4696.
7 C. H. Schiesser, H. Matsubara, I. Ritsner and U. Wille, *Chem. Commun.*, 2006, 1067.
8 H. Matsubara, C. T. Falzon, I. Ryu and C. H. Schiesser, *Org. Biomol. Chem.*, 2006, **4**, 1920.
9 I. Ryu, K. Matsu, S. Minakata and M. Komatsu, *J. Am. Chem. Soc.*, 1998, **120**, 5838; M. Tojino, N. Otsuka, T. Fukuyama, H. Matsubara and I. Ryu, *J. Am. Chem. Soc.*, 2006, **128**, 7712.
10 A. L. J. Beckwith and C. H. Schiesser, *Tetrahedron*, 1985, **41**, 3925; D. C. Spellmeyer and K. N. Houk, *J. Org. Chem.*, 1987, **52**, 959.
11 For a review see: C. H. Schiesser, U. Wille, H. Matsubara and I. Ryu, *Acc. Chem. Res.*, 2007, **40**, 303.
12 M. Mohr, H. Zipse, D. Marx and M. Parrinello, *J. Phys. Chem. A*, 1997, **101**, 8942.
13 S. L. Boyd and R. J. Boyd, *J. Phys. Chem. A*, 2001, **105**, 7096.
14 *Gaussian 03*, Revision B.04, M. J. Frisch, G. W. Trucks, H. B. Schlegel, G. E. Scuseria, M. A. Robb, J. R. Cheeseman, J. A. Montgomery, Jr., T. Vreven, K. N. Kudin, J. C. Burant, J. M. Millam, S. S. Iyengar, J. Tomasi, V. Barone, B. Mennucci, M. Cossi, G. Scalmani, N. Rega, G. A. Petersson, H. Nakatsuji, M. Hada, M. Ehara, K. Toyota, R. Fukuda, J. Hasegawa, M. Ishida, T. Nakajima, Y. Honda, O. Kitao, H. Nakai, M. Klene, X. Li, J. E. Knox, H. P. Hratchian, J. B. Cross, C. Adamo, J. Jaramillo, R. Gomperts, R. E. Stratmann, O. Yazyev, A. J. Austin, R. Cammi, C. Pomelli, J. W. Ochterski, P. Y. Ayala, K. Morokuma, G. A. Voth, P. Salvador, J. J. Dannenberg, V. G. Zakrzewski, S. Dapprich, A. D. Daniels, M. C. Strain, O. Farkas, D. K. Malick, A. D. Rabuck, K. Raghavachari, J. B. Foresman, J. V. Ortiz, Q. Cui, A. G. Baboul, S. Clifford, J. Cioslowski, B. B. Stefanov, G. Liu, A. Liashenko, P. Piskorz, I. Komaromi, R. L. Martin, D. J. Fox, T. Keith, M. A. Al-Laham, C. Y. Peng, A. Nanayakkara, M. Challacombe, P. M. W. Gill, B. Johnson, W. Chen, M. W. Wong, C. Gonzalez and J. A. Pople, Gaussian, Inc., Pittsburgh PA, 2003.
15 *NBO 5.0*, E. D. Glendening, J. K. Badenhoop, A. E. Reed, J. E. Carpenter, J. A. Bohmann, C. M. Morales and F. Weinhold, Theoretical Chemistry Institute, University of Wisconsin, Madison, 2001.
16 I. Beranek and H. Fischer, *NATO ASI Ser., Ser. C*, 1989, **260**, 303.